A new complex intermetallic phase in the system Al-Cu-Ta with familiar clusters and packing principles

Journal Article

Author(s):
Dshemuchadse, J.; Bigler, S.; Simonov, Arkadiy (iD); Weber, T.; Steurer, W.

A new complex intermetallic phase in the system Al–Cu–Ta with familiar clusters and packing principles

Julia Dshemuchadse, Sandro Bigler, Arkadiy Simonov, Thomas Weber and Walter Steurer

Acta Crystallographica Section B: Structural Science publishes papers in structural chemistry and solid-state physics in which structure is the primary focus of the work reported. The central themes are the acquisition of structural knowledge from novel experimental observations or from existing data, the correlation of structural knowledge with physico-chemical and other properties, and the application of this knowledge to solve problems in the structural domain. The journal covers metals and alloys, inorganics and minerals, metal-organics and purely organic compounds.

Crystallography Journals Online is available from **journals.iucr.org**

A new complex intermetallic phase in the system Al–Cu–Ta with familiar clusters and packing principles

Julia Dshemuchadse,* Sandro Bigler, Arkadiy Simonov, Thomas Weber and Walter Steurer*

Laboratory of Crystallography, Department of Materials, ETH Zurich, Wolfgang-Pauli-Strasse 10, 8093 Zurich, Switzerland

Correspondence e-mail:
julia.dshemuchadse@mat.ethz.ch,
steurer@mat.ethz.ch

The structure of $hP386$-$Al_{57.4}Cu_{3.6}Ta_{39.0}$ was determined by single-crystal X-ray diffraction analysis. It can be described as a hexagonal close-packing of two types of endohedral fullerene-like clusters with different Frank–Kasper polyhedra filling the gaps. The description of the structure as a superstructure and as a layered structure illustrates other characteristic structural building principles. The diffuse scattering, which can be observed in some of the crystals, is qualitatively well reproduced by a disorder model. A comparison with the structures of the other complex intermetallics in the system Al–Cu–Ta indicates the decisive role that Cu plays in the constitution and packing of the clusters.

1. Introduction

Recently, it has been shown that cluster-based face-centered cubic (f.c.c.) intermetallics with large unit cells can be described in a rather unified way, although they differ greatly in chemical composition and bonding (Dshemuchadse *et al.*, 2011). The complex structures resulting from certain stoichiometries can be seen as a compromise between the formation of low-energy structural subunits – our 'clusters' (Steurer, 2006) – and their densest possible packing. This indicates the dominating role of topological building principles.

In the system Al–Cu–Ta there is a bundle of complex intermetallic phases with only slightly differing compositions consisting of essentially the same types of clusters: the hexagonal compound $hP386$ (as mentioned in Weber *et al.*, 2009) with the refined composition $Al_{57.4}Cu_{3.6}Ta_{39.0}$ and the f.c.c. phases $cF444$-$Al_{63.6}Ta_{36.4}$ (Mahne & Harbrecht, 1994; Weber *et al.*, 2009), $cF(5928-20)$-$Al_{56.6}Cu_{3.9}Ta_{39.5}$ and $cF(23256-122)$-$Al_{55.4}Cu_{5.4}Ta_{39.2}$ (Weber *et al.*, 2009; Conrad *et al.*, 2009). As we will show in the following, the previously unknown structure of $hP386$-$Al_{57.4}Cu_{3.5}Ta_{39.0}$ is closely related to that of $hP390$-$Na_{49.2}In_{49.8}Ni_{1.0}$ (Sevov & Corbett, 1993*a*).

2. Structure determination

The structure of $hP386$-$Al_{57.4}Cu_{3.6}Ta_{39.0}$ was determined by standard single-crystal X-ray diffraction analysis, as described in the following.

2.1. Experimental

Samples with nominal composition $Al_{56}Cu_4Ta_{40}$ (Al: 99.9999%, Cu: 99.9999%, Ta: 99.995%) were molten in an arc furnace under argon atmosphere for homogenization. During this step, 0.8 wt % of the material was lost due to evaporation. The resulting pre-alloy was then placed in an Al_2O_3 crucible,

electronic reprint

Table 1
Experimental details.

Crystal data	
Chemical formula	$Al_{220.86}Cu_{13.70}Ta_{150}$
M_r	33 971.80
Crystal system, space group	Hexagonal, $P6_3/mmc$
Temperature (K)	293
a, c (Å)	13.5120 (18), 39.022 (5)
V (Å^3)	6169.9 (14)
Z	1
Radiation type	Mo $K\alpha_1$
μ (mm^{-1})	68.10
Crystal size (mm)	$0.05 \times 0.04 \times 0.03$
Data collection	
Diffractometer	MAR300 image plate
Absorption correction	Multi-scan *XDS*
T_{min}, T_{max}	0.132, 0.235
No. of measured, independent and observed [$I > 2\sigma(I)$] reflections	86 727, 2608, 2556
R_{int}	0.072
$(\sin \theta/\lambda)_{max}$ (Å^{-1})	0.641
Refinement	
$R[F^2 > 2\sigma(F^2)]$, $wR(F^2)$, S	0.029, 0.063, 1.22
No. of reflections	2608
No. of parameters	137
No. of restraints	0
$\Delta\rho_{max}$, $\Delta\rho_{min}$ (e Å^{-3})	3.33, −2.74

Computer programs: *XDS* (Kabsch, 1993), *SUPERFLIP* (Palatinus & Chapuis, 2007), *SHELXL*97 (Sheldrick, 2008), *CrystalMaker* (CrystalMaker Software Ltd, 2009).

sealed in a tantalum ampoule under an argon atmosphere and subsequently heated up to 1773 K with a heating rate of 400 K h^{-1}. The sample was kept at this temperature for 56 h, also in an argon atmosphere, and then quenched in water. Differential thermal analysis showed that the compound melts congruently at 1873 (16) K. Its composition was determined by electron microprobe analysis to be $Al_{58.6\,(1)}Cu_{4.1\,(1)}Ta_{37.3\,(2)}$.

The single-crystal X-ray diffraction data were collected in-house using a rotating anode X-ray source and a MAR300 imaging-plate detector. For further experimental details see Table 1. Some single crystals selected from the same sample show diffuse streaks in the **c*** direction through strong Bragg reflections, indicating stacking faults or polytypic disorder. The structure analysis presented below refers to a data collection on a sample without these features. The refined model, however, was also tested with a dataset recorded on a sample exhibiting diffuse streaks and could be confirmed. Details on the disordered structure are discussed below.

2.2. Refinement

The structure was solved by the charge-flipping method (Palatinus & Chapuis, 2007) and refined in the space group $P6_3/mmc$. Although – as usual for complex intermetallic compounds – a significant degree of disorder is found in this structure, 15 out of 16 Ta positions and 10 out of 14 Al positions are fully ordered. The remaining Ta atom as well as three Al atoms are located on split positions and one Al position is deficient. Furthermore, all Cu atoms are found on mixed Al/Cu sites, occupying them to an extent between 5 and 39%.

The atomic displacement parameters (ADPs) were refined anisotropically only for the ordered Ta sites. The ADPs of the split Ta position are considered to be isotropic in order to avoid too strong correlations. For the same reason all Al sites were regarded to have the same (isotropic) ADP and the mixed Al/Cu sites are assigned one common isotropic ADP as well. The interatomic distances are physically reasonable. The relatively short Al—Al (2.48 Å) and Ta—Ta distances (2.58 Å) are not uncommon in complex intermetallics and are in some cases regarded as reflecting partly covalent bonding.

Note that the refined composition $Al_{57.4\,(1.1)}Cu_{3.6\,(2)}Ta_{39.0\,(5)}$ slightly deviates from that determined by electron microprobe. This has to be accepted for an intermetallic compound of this complexity with a significant amount of disordered atomic sites.

3. Cluster descriptions

The description of structures with building blocks, called 'clusters', has become a popular way to treat intermetallic structures of different kinds, *e.g.* quasicrystals (Steurer, 2006) or periodic compounds with large unit cells (Dshemuchadse *et al.*, 2011). If the chemical bonding in a structure is not analyzed in detail, this is mainly a geometric discussion. Since cluster descriptions can be ambiguous and the ideal interpretation of atomic positions by clusters is not always obvious, we discuss three different approaches below.

3.1. Structure description based on three-shell clusters

Two slightly different three-shell clusters are found around two Wyckoff sites of highest symmetry: 2a and 2c.[1] All cluster shells are depicted in Fig. 1 and the contributing atoms are listed in Table 2.

The first cluster shell around the vacant 2a site is formed by a Ta_2Al_6 rhombohedron, which can adopt six different orientations. This disordered shell is surrounded by a pentagon–dodecahedron of Ta atoms with the pentagon faces all capped by split Al atoms,[2] resulting in a distorted rhombic triacontahedron, $Al_{12}Ta_{20} – FK_{32}^{60}$ (FK_V^F designating a Frank–Kasper polyhedron with F faces and V vertices (Dshemuchadse *et al.*, 2011). The third cluster shell has the shape of a F_{60}^{32} fullerene-like polyhedron (F_V^F designating a fullerene with F faces and V vertices, dual to the Frank–Kasper polyhedron FK_V^F; Dshemuchadse *et al.*, 2011), consisting of 12 Ta, 18 Al and 30 mixed Al/Cu positions. Remarkably, the 12 Ta atoms form, together with 6 Al atoms, a staggered ring perpendicular to the [001] direction – an 'equatorial ring'. It contains Ta–Ta dimers with distance $d_{Ta-Ta} = 2.583$ Å, the shortest found for Ta—Ta in this compound, while the Al—Ta distances range between 2.802 and 2.809 Å. There are no Cu atoms next to the Ta atoms. The mixed Cu-containing posi-

---

[1] Site 2a: 0, 0, 0 and 0, 0, $\frac{1}{2}$, site symmetry $\bar{3}m$.; site 2c: $\frac{1}{3}$, $\frac{2}{3}$, $\frac{1}{4}$ and $\frac{2}{3}$, $\frac{1}{3}$, $\frac{3}{4}$, site symmetry $\bar{6}m2$.
[2] The heavily disordered atoms sit in neighboring cluster shells and are correlated. Al07b cannot be occupied by an atom when the closest Al06a/b sites are occupied and analogously Al09b cannot be occupied when an atom is located on the closest Ta09a/b sites.
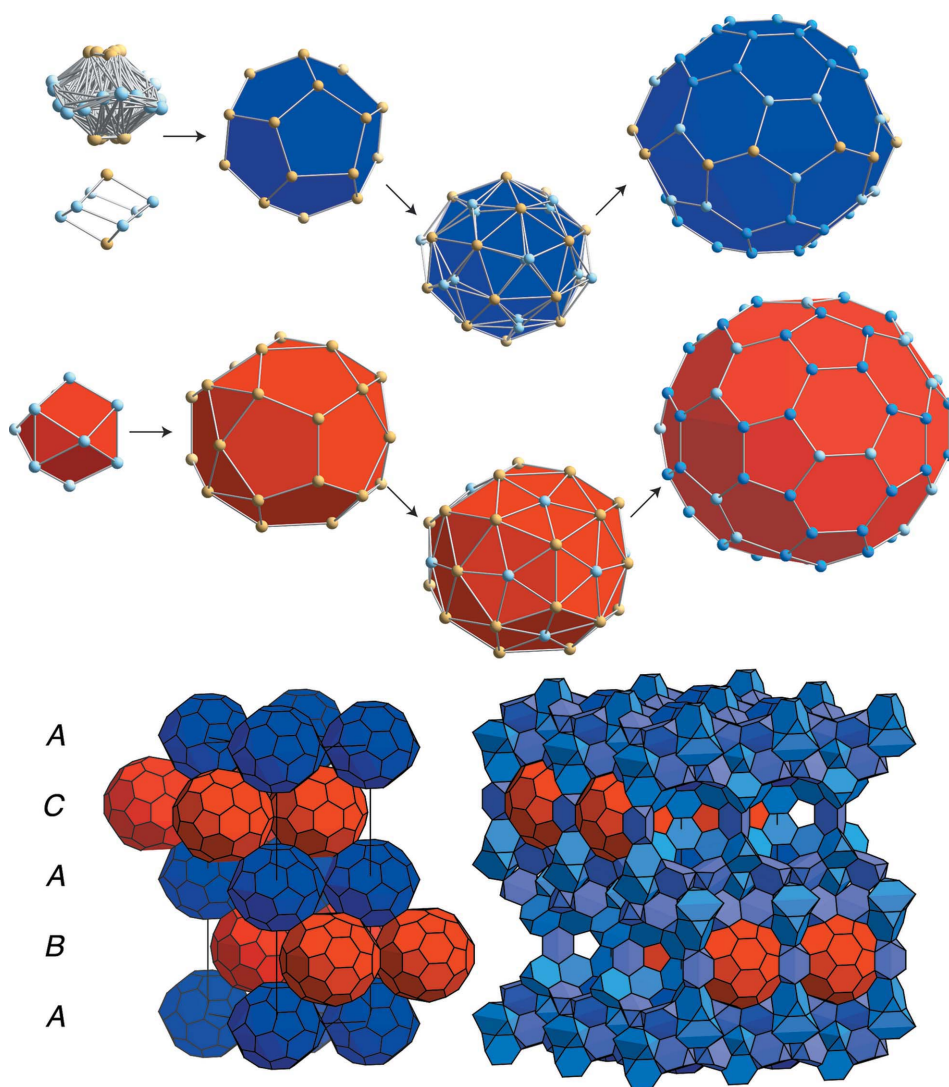
Figure 1
Clusters in $hP386$-$Al_{57.4}Cu_{3.6}Ta_{39.0}$. Light blue, blue and brown colored atoms correspond to Al, Al/Cu and Ta sites, respectively. The three shells of the F_{60}^{32} cluster are shown on the *top* (blue polyhedra) and those of the F_{74}^{39} cluster in the *middle* (red polyhedra). The packing of the clusters is shown *below*: on the *left* $ABAC$ stacking in the **c** direction is shown, where A layers are comprised of differently oriented F_{60}^{32} clusters (blue) and B and C layers of F_{74}^{39} clusters (red). The full packing is depicted on the *right*, where also the intermediate clusters FK_{16}^{28} and FK_{15}^{26} in light blue and violet, respectively, are visualized.

The radii of the F_{60}^{32} and F_{74}^{39} polyhedra are in the range 6.2–6.9 and 6.3–7.2 Å, respectively. The F_{60}^{32} clusters are arranged in hexagonal close-packed (h.c.p.) layers perpendicular to [001] and share Ta–Ta edges along the 'equatorial ring' of Ta atoms. The F_{74}^{39} clusters build h.c.p. layers by sharing half of their pentagonal faces. Their other six pentagonal faces are shared with the F_{60}^{32} clusters in the h.c.p. layers above and below.

Similarly, each F_{60}^{32} cluster is connected with six F_{74}^{39} polyhedra (three above and three below) by shared pentagonal faces. If the h.c.p. layers, constituted by F_{60}^{32}- and F_{74}^{39} clusters, are referred to as A and B/C layers, respectively, the cluster structure can be regarded as an $ABAC$ stacking sequence. It is important to note that not only are different clusters featured in the A and B/C layers, but also the clusters in the first and second A layers, as well as the B and C layers have different orientations. The abstract stacking sequence corresponds to that of the $hP4$-NiAs structure type (see Fig. 1).

The interstices between the fullerene clusters are filled by the Frank–Kasper polyhedra FK_{15}^{26} and FK_{16}^{28} (CN15 and CN16, respectively, the latter being a Friauf polyhedron; Frank & Kasper, 1958). Two peculiarities of the cluster packing have to be mentioned: one is a small tetrahedron-shaped void formed by two FK_{16}^{28} and two FK_{15}^{26} clusters; another is found at the pentagonal faces of the F_{60}^{32} clusters, which are not shared with other fullerene-like polyhedra but are interpenetrated by one type of FK_{16}^{28}. These Friauf polyhedra are sharing atoms with inner shells of the neighboring F_{60}^{32} clusters.

tions thus only have Al atoms and other Al/Cu sites as neighbors within the shell and are found on the 'north and south poles' of the F_{60}^{32} cluster with respect to the 'equatorial ring' of Ta atoms.

The other highly symmetric Wyckoff position 2c is occupied by Ta, which then is surrounded by an Al_{11} coordination polyhedron of trigonal symmetry, which contains the only deficient Al position in this compound. The second cluster shell can be described as a Ta_{27} polyhedron, consisting of 12 pentagonal and 14 triangular faces; all pentagons are capped by Al atoms, resulting in a FK_{39}^{74} polyhedron with composition $Al_{12}Ta_{27}$. The third cluster shell has the shape of a F_{74}^{39} fullerene and consists of 20 Al and 54 mixed Al/Cu positions. All Al/Cu sites contained in the structure are part of this shell.

3.2. The Ta framework

Another view on the structure of $hP386$-$Al_{57.4}Cu_{3.6}Ta_{39.0}$ can be obtained by depicting the framework constituted by the Ta atoms (Fig. 2; for cluster details see Table 2). The Ta pentagon–dodecahedron and the Ta_{27} polyhedron, *i.e.* the second cluster shells around the 2a and 2c positions, have

Table 2
Details of the clusters in $hP386$-$Al_{57.4}Cu_{3.6}Ta_{39.0}$.

Given are the clusters of the network of fullerenes and FK polyhedra (upper part), as well as the Ta network (middle part) and the network of icosahedra (all FK_{12}^{20}, with $r \simeq 4.0$ Å) (lower part).

Shell	Shape	Wyckoff site		Atoms
0th	Central site	2a	0, 0, 0	Empty
1st	Rhombohedron		$r \simeq 3.0$ Å	2 × Ta09a/b (six-fold split), 6 × Al06 (three-fold split)
2nd	F_{20}^{12}		$r \simeq 5.0$ Å	2 × Ta03, 6 × Ta11, 12 × Ta15
+ caps	FK_{32}^{60}			6 × Al07a/b, 6 × Al09a/b
3rd	F_{60}^{32}		$r \simeq 7.0$ Å	12 × Ta08, 6 × Al08, 12 × Al10, 6 × Al/Cu1, 12 × Al/Cu2, 12 × Al/Cu3
0th	Central site	2c	1/3 , 2/3, 1/4	Ta01
1st	'FK'$_{11}$		$r \simeq 4.0$ Å	2 × Al02, 3 × Al04 (deficient), 6 × Al14
2nd	'F_{27}^{26}		$r \simeq 6.0$ Å	3 × Ta07, 6 × Ta12, 6 × Ta14, 12 × Ta16
+ caps	FK_{39}^{74}			6 × Al05, 6 × Al12
3rd	F_{74}^{39}		$r \simeq 7.5$ Å	2 × Al01, 6 × Al03, 6 × Al11, 6 × Al13, 6 × Al/Cu1, 12 × Al/Cu2, 12 × Al/Cu3, 12 × Al/Cu4, 12 × Al/Cu5
0th	Central site	2d	1/3, 2/3, 3/4	Ta02
1st	FK_{15}^{26}		$r \simeq 4.0$ Å	6 × Al13, 6 × Al/Cu5; caps: 3 × Ta07
0th	Central site	4e	0, 0, z	Ta04
1st	FK_{16}^{28}		$r \simeq 4.0$ Å	3 × Al03, 6 × Al/Cu3, 3 × Al/Cu4; caps: 1 × Ta03, 3 × Ta14
0th	Central site	4f	1/3, 2/3, z	Ta05
1st	FK_{16}^{28}		$r \simeq 4.0$ Å	3 × Al07a/b, 3 × Al08, 6 × Al10; caps: 1 × Ta06, 3 × Ta08
0th	Central site	4f	1/3, 2/3, z	Ta06
1st	FK_{16}^{28}		$r \simeq 4.0$ Å	6 × Al10, 3 × Al11, 3 × Al13; caps: 1 × Ta05, 3 × Ta13
0th	Central site	12k	x, 2x, z	Ta10
1st	FK_{15}^{26}		$r \simeq 4.0$ Å	2 × Ta08, 1 × Al01, 2 × Al08, 2 × Al10, 1 × Al11, 2 × Al/Cu1, 2 × Al/Cu2; caps: 1 × Ta12, 2 × Ta15
0th	Central site	12k	x, 2x, z	Ta13
1st	FK_{16}^{28}		$r \simeq 4.0$ Å	2 × Al10, 2 × Al11, 2 × Al13, 2 × Al/Cu2, 2 × Al/Cu3, 1 × Al/Cu4, 1 × Al/Cu5; caps: 1 × Ta06, 1 × Ta11, 2 × Ta16

Shell	Shape	Wyckoff site		Atoms
0th	Central site	4f	1/3, 2/3, z	Ta05
1st	FK_{16}^{28}		$r \simeq 4.0$ Å	3 × Al07a/b, 3 × Al08, 6 × Al10; caps: 1 × Ta06, 3 × Ta08
2nd	F_{28}^{16}		$r \simeq 5.5$ Å	6 × Ta10, 3 × Ta11, 3 × Ta13, 12 × Ta15, 1 × Al01, 3 × Al11

Table 2 (continued)

Shell	Shape	Wyckoff site		Atoms
0th	Central site	6g	1/2, 0, 0	Empty
1st	Hexagonal bipyramid		$r \simeq 3.0$ Å	2 × Ta10, 4 × Ta15; caps: 2 × Ta08
0th	Central site	6h	$x, \bar{x}, 1/4$	Empty ($x = 0.8457$)
1st	Pentagonal bipyramid		$r \simeq 3.0$ Å	1 × Al03, 2 × Al/Cu4, 2 × Al/Cu5; caps: 2 × Al05
2nd	Pentagonal bifrustum		$r \simeq 4.5$ Å	1 × Ta02, 2 × Ta04, 2 × Ta07, 2 × Ta13, 4 × Ta14, 4 × Ta16
0th	Central site	12k	x, 2x, z	Empty ($x = 0.1426$, $z = 0.1109$)
1st	Pentagonal bipyramid		$r \simeq 3.0$ Å	1 × Al/Cu1, 2 × Al/Cu2, 2 × Al/Cu3; caps: 1 × Al09a/b, 1 × Al12
2nd	Pentagonal bifrustum		$r \simeq 4.5$ Å	1 × Ta03, 1 × Ta04, 2 × Ta10, 2 × Ta11, 2 × Ta12, 2 × Ta13, 1 × Ta14, 2 × Ta15, 2 × Ta16

Center	Atoms
Al01	3 × Al08, 3 × Al/Cu1, 3 × Ta10, 3 × Ta12
Al03	2 × Al03, 2 × Al05, 2 × Al/Cu4, 2 × Ta04, 4 × Ta14
Al08	1 × Al01, 1 × Al07a/b, 2 × Al08, 1 × Al/Cu1, 1 × Ta05, 2 × Ta08, 2 × Ta10, 2 × Ta15
Al10	1 × Al07a/b, 2 × Al10, 1 × Al11, 1 × Al/Cu2, 1 × Ta05, 1 × Ta06, 1 × Ta08, 1 × Ta10, 1 × Ta11, 1 × Ta13, 1 × Ta15
Al11	2 × Al10, 1 × Al13, 2 × Al/Cu2, 1 × Ta06, 1 × Ta10, 1 × Ta12, 2 × Ta13, 2 × Ta16
Al13	1 × Al11, 2 × Al13, 2 × Al/Cu5, 1 × Ta02, 1 × Ta06, 1 × Ta07, 2 × Ta13, 2 × Ta16
Al/Cu1	1 × Al01, 1 × Al08, 1 × Al09a/b, 1 × Al12, 2 × Al/Cu2, 2 × Ta10, 2 × Ta12, 2 × Ta15
Al/Cu2	1 × Al09a/b, 1 × Al10, 1 × Al11, 1 × Al12, 1 × Al/Cu1, 1 × Al/Cu3, 1 × Ta10, 1 × Ta11, 1 × Ta12, 1 × Ta13, 1 × Ta15, 1 × Ta16
Al/Cu3	1 × Al09a/b, 1 × Al12, 1 × Al/Cu2, 2 × Al/Cu3, 1 × Al/Cu4, 1 × Ta03, 1 × Ta04, 1 × Ta11, 1 × Ta13, 1 × Ta14, 1 × Ta16
Al/Cu4	1 × Al03, 2 × Al05, 2 × Al/Cu3, 1 × Al/Cu5, 1 × Ta04, 1 × Ta13, 2 × Ta14, 2 × Ta16
Al/Cu5	2 × Al05, 2 × Al13, 1 × Al/Cu4, 1 × Al/Cu5, 1 × Ta02, 2 × Ta07, 1 × Ta13, 2 × Ta16

already been discussed above. In addition, a F_{28}^{16} fullerene-like cluster is found around another Ta atom,[3] with hexagonal bipyramids formed by three of its four hexagon faces. The interatomic distances of the two Ta atoms at the apices of the bipyramid are the shortest Ta—Ta distances in the compound (2.583 Å) as is the case for hexagonal bipyramids found in the related f.c.c. Al–Cu–Ta structures (Conrad *et al.*, 2009).

The spaces between these three kinds of clusters are filled with pentagonal Ta_{15} bifrusta, centered by Al_7 pentagonal bipyramids. These clusters have also been found in the cubic Al–Cu–Ta compounds (Conrad *et al.*, 2009). The bifrusta are sharing pentagonal faces with the second-shell F_{20}^{12} and F_{27}^{26} clusters. All 12 pentagonal faces of the latter cluster are covered like this leaving only the 14 triangular faces open, while the former cluster – the pentagon-dodecahedron –

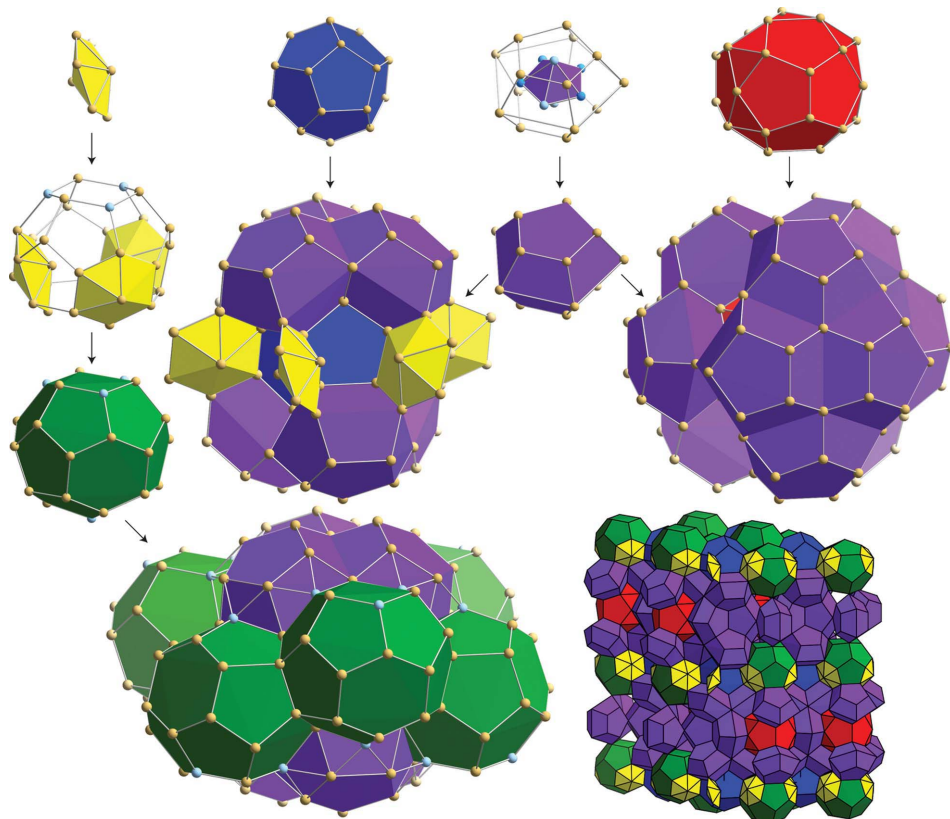[3] Ta05, $4f$ $\frac{1}{3}, \frac{2}{3}, z$ with $z = 0.53716$.

Figure 2
Clusters of the Ta network in $hP386$-$Al_{57.4}Cu_{3.6}Ta_{39.0}$. On the *top*, the second cluster shells around $2a$ and $2c$ are shown in blue and red. In the *top middle* a pentagonal Ta-bifrustum and its inner pentagonal bipyramid (purple) are depicted. The arrangement of these bifrusta around $2a$ and $2c$ positions is shown *below* and at the far *left* the F_{28}^{16} polyhedron (green) is shown with hexagonal bipyramids (yellow) on three of its four hexagonal faces. The packing of all these polyhedra is shown in the *lower right*.
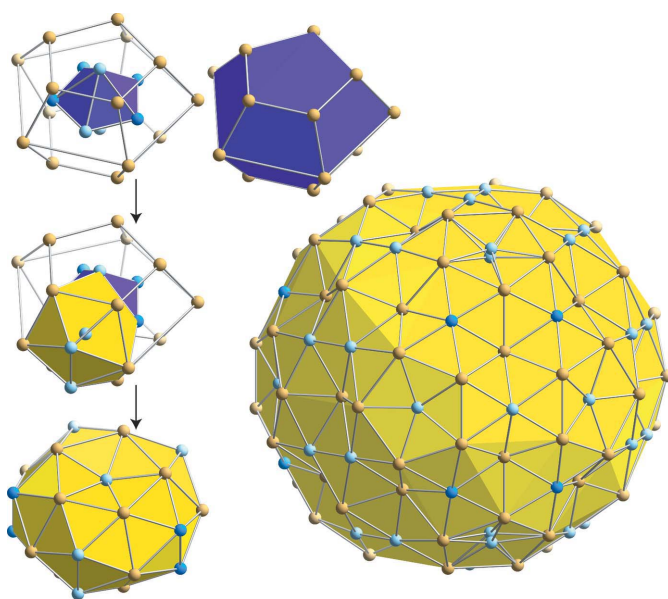

Figure 3
Network of icosahedra in $hP386$-$Al_{57.4}Cu_{3.6}Ta_{39.0}$. On the *left* the pentagonal Ta-bifrustum centered by a pentagonal bipyramid is shown, as well as its assembly by five icosahedra. Transferring this principle to all Ta-bifrusta, as well as the remaining positions in the fullerene-like cluster shells, a mantle of partially interpenetrating icosahedra around sites $2a$ (not shown) and $2c$ (*right*) can be found.

shares 6 of its 12 pentagonal faces with bifrusta. It has the remaining ones in common with the F_{28}^{16} clusters, which in turn share hexagonal faces amongst themselves and complete the packing of the unit cell.

3.3. A network of icosahedra

As mentioned before, the packing of the two fullerene-like three-shell clusters is supplemented with FK_{16}^{28} and FK_{15}^{26} polyhedra to fill the unit cell. These and similar higher coordinations were found around most Ta positions, while many Al and Al/Cu sites are surrounded by icosahedra or polyhedra with similar coordination numbers. This can be most strikingly shown on the third-shell clusters at the $2a$ and $2c$ sites: all 11 different Al and Al/Cu atoms in the fullerene-like clusters are coordinated by FK_{12}^{20} shells, *i.e.* icosahedra, while the only Ta position exhibits a FK_{14}^{24} coordination.

Simultaneously to being part of the outer shells in the description with three-shell clusters, these atomic positions can also be regarded in light of the Ta network. They belong to the basal plane of the pentagonal bipyramids within the bifrusta. These pentagons of the third-shell cluster are therefore sitting exactly opposite the pentagons of the second cluster shell made of Ta atoms, but in an inverted orientation. Each of the sites in the third cluster shell is the center of an icosahedron, resulting in a full covering of the shell by icosahedra around $2c$, as shown in Fig. 3. The Ta atoms in the cluster shell around $2a$ are the only sites in the two third-shell clusters that do not have icosahedral coordination. Therefore, an imperfect shell of icosahedra results around $2a$.

If all atoms constituting those icosahedra – as central or vertex atoms – are considered, the only sites not described by this network of icosahedra are those building the first-shell clusters of the two fullerenes at sites $2a$ and $2c$.[4]

4. Diffuse scattering

As mentioned above, samples of this new Al–Cu–Ta phase contained single crystals both with and without significant diffuse scattering. The structure model explained above was

---

[4] The sites, which are not described by the network of 11 symmetrically inequivalent icosahedra, are Al02, Al04, Al06, Al14, Ta01 and Ta09.
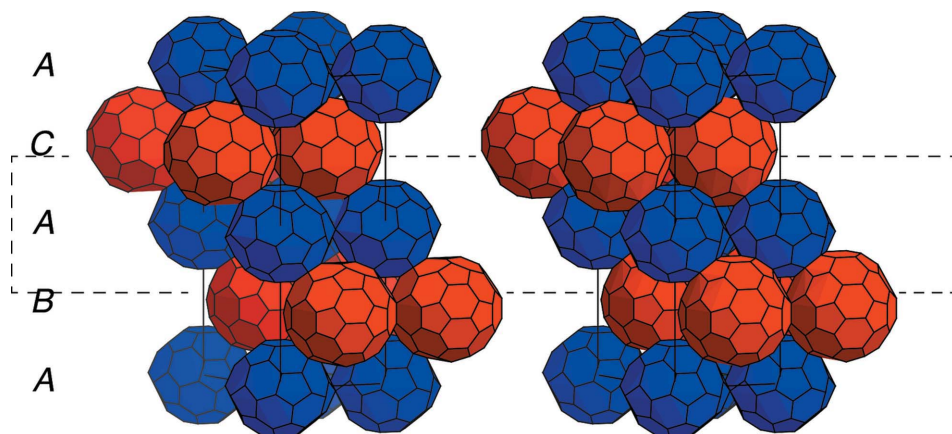
Figure 4
Two different disordered cluster structures in $hP386$-Al$_{57.4}$Cu$_{3.6}$Ta$_{39.0}$. The original unit cell (*left*), as well as the one with an exchanged slab (*right*), both exhibiting $ABAC$ stacking in the **c** direction. The volume affected by disorder is indicated by the dashed-line box. The A layers are comprised of F_{60}^{32} clusters in both cases (blue), while the B and C layers in the original case are F_{74}^{39} clusters, but in the disordered variant they are found to be F_{76}^{40} clusters (all red), because the adjacent layer of F_{60}^{32} clusters in the center of the unit cell is exchanged.

coordinates $x, y, 1 - z$ derived from Ta atoms at x, y, z. Consequently, these maxima are assigned to be Ta positions of the disordered structure. Additional positions close to the borders of this slab were also assigned mirrored coordinates until a chemically reasonable model could be achieved. This concerns most atoms in this part of the unit cell,[5] except for the extremely disordered first cluster shell of the F_{60}^{32} cluster at $0, 0, \frac{1}{2}$, because this structure motif was originally already close to being mirror-symmetric and had such a smeared-out electron density that its mirroring would have had basically no effect at all.

The unit cell of the disordered structural variant is shown in Fig. 4 with the changed atomic positions in the central slab; the rest of the unit cell features the same atomic positions as the ordered structure model. The effect on the cluster structure is the following: the layers of F_{60}^{32} clusters with centers at $z = 0$ and $z = 1$ are unchanged, but the F_{60}^{32} clusters at $z = \frac{1}{2}$ are mirrored with respect to the ordered structure. The other fullerene-like clusters, however, are 'cut apart' and 're-glued' in a different manner, which results in a different number and arrangement of atoms per cluster: where F_{74}^{39} clusters were found in the ordered structure, the disorder model features F_{76}^{40} – the same cluster that was found in all three cubic Al–(Cu)–Ta compounds (Conrad *et al.*, 2009).

The diffuse scattering that should arise from the modeled disorder was calculated with the program *Yell* (Simonov *et al.*, 2013). The calculated diffuse scattering corresponds to zero-neighbor correlations only. This means that we disregard possible interactions of disordered layers with each other within the structure. We do so for two reasons: (1) disordered slabs are rare in the structure ($\sim 5\%$, see above) and are therefore unlikely to interact with one another, and (2) Bragg scattering and diffuse streaks overlap, concealing any possible fine structure; therefore, we assume a broad shape of the diffuse intensities in the following.

Reconstructions of the diffuse scattering are shown in Fig. 5 for the $h0l$ plane and in Fig. 6 for the $h5l$ plane. The background intensity of the images was approximated by the average value of the intensities measured above and below the reconstructed layers (in the perpendicular direction, *i.e.* **b*** for the $h0l$ plane, at points $h\frac{1}{4}l$ and $h\frac{1}{4}l$). The diffraction patterns contain sharp streaks along the **c*** direction in rows of Bragg peaks. This means that the disordered part of the structure is well ordered in the **ab** plane, with the same periodicity as the

obtained from a sample which did not show structured diffuse intensities; therefore we will subsequently call it the ordered structure model.

Another crystal, exhibiting diffuse scattering and therefore containing correlated disorder, was also measured completely and its structure will now be compared with the ordered model. Unfortunately, to measure the diffuse intensities the crystal had to be larger than optimal to collect Bragg data. This gave rise to absorption effects which impair the resulting diffraction data. Furthermore, the Bragg reflections heavily overlap with the diffuse scattering intensities. For both these reasons, the refinement of the ordered model against this second dataset cannot yield fully unbiased parameters. However, we observe a number of additional electron density peaks when performing one refinement cycle with the ordered model on the dataset of the disordered structure. In the following these peaks will be interpreted as atomic positions of the disordered structure: they correspond to a much lower occupancy than the positions from the ordered model with a weighting of approximately 5:95. Another characteristic of the disordered structure is that the ADPs are larger in the **c** direction. This could either be an artifact from absorption effects or a hint towards a physical difference between ordered and disordered structures.

The discrepancies between the ordered and the disordered structures can be examined better when a difference electron density is considered. For this we computed the difference structure factor $(|F_{\text{ordered}}| - |F_{\text{disordered}}|) \times e^{i\varphi_{\text{ordered}}}$ and from it – by Fourier transformation – the difference electron density. This can be more easily interpreted than the refinement of the flawed dataset of the disordered structure, and our model for the structural disorder is derived from these observations.

The majority of all difference maxima can be found in a central slab of structure around $x, y, \frac{1}{2}$ with $\Delta z \simeq \pm 0.16$. The maxima appear to be mirror images of Ta positions with

---

[5] The flipped atoms were the following: Ta05, Ta06, Ta08, Ta10, Ta11, Ta13, Ta15, Al01, Al07a/b, Al08, Al09a/b, Al10, Al12, Al/Cu1, Al/Cu2, Al/Cu3.

average structure. The fact that the diffuse features are very broad in the $\mathbf{c}^*$ direction on the other hand means that the correlation length of local order is much smaller than the length of the $\mathbf{c}$ axis.[6]

The computed diffuse scattering intensities are very similar to the experimentally measured ones. However, the modeled diffuse intensity decayed much slower in the $\mathbf{c}^*$ direction than the experimental one. This characteristic is linked with the ADP parameters, which therefore should assume larger values in the U^{33} component. As mentioned earlier, a corresponding effect was observed for the refinement of the ordered structure model against the disordered structure data. To account for this property of the average structure of the dataset, we increased the ADP components U^{33} for all disordered atoms by 0.02 Å^2. Apart from this adjustment all atomic parameters were derived directly from the ordered model and the difference electron density as described, without any refinement against the diffuse scattering.

The final model reproduces the variation of the diffuse scattering very nicely. It is essentially a zero-parameter model in the sense that no parameters were refined to fit the diffuse scattering. This means that although the observed diffuse scattering is intrinsically difficult to measure and therefore also to evaluate – due to the overlap with Bragg reflections – the good match of the experimental and calculated diffraction patterns suggests that the model should be essentially correct.

The disorder in this intermetallic structure does not take a classical form: stacking faults frequently occur in the form of domain boundaries, causing diffuse streaks in between rows of Bragg reflections. Here an intermediate slab of structure is replaced in a mainly ordered matrix. This unusual 'inlet' structure represents an additional degree of freedom. It corresponds to a structural variant that is possible but unlikely to occur.

5. Discussion

5.1. Superstructure description

Most structures of complex intermetallics can be described as superstructures of simpler basic structures that are related to a subset of strong Bragg reflections (Dshemuchadse *et al.*, 2011). In the case of $hP386$-Al$_{57.4}$Cu$_{3.6}$Ta$_{39.0}$, in the $hk0$ plane the strong 330 reflection and its symmetrically equivalents form such a subset. Thus we can interpret our complex structure to be a (3×3)-fold superstructure of an underlying simple basic structure along [100] and [010]. In the $h0l$ set of reflections, which remarkably shows decagonal pseudo-symmetry, the most prominent reflections are $30\overline{14}$ and $00\overline{28}$ (not shown), as well as their symmetry equivalents (see Fig. 7). As a consequence, the lattice parameter a_B of the basic structure is $1/3$ of the lattice parameter a of $hP386$-Al$_{57.4}$Cu$_{3.6}$Ta$_{39.0}$ and c_B results in $1/14$ or $1/28$ of c. The resulting average structures are depicted in Fig. 8. In the

---

[6] Supplementary data for this paper are available from the IUCr electronic archives (Reference: SN5123). Services for accessing these data are described at the back of the journal.
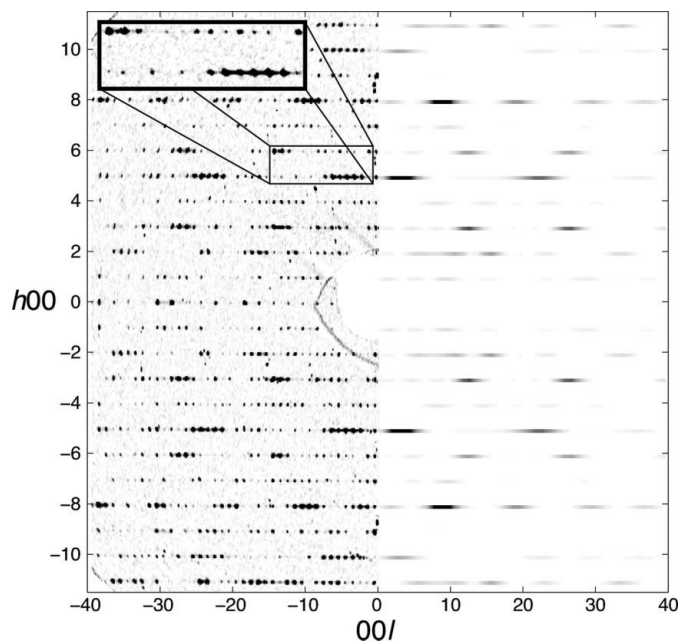

Figure 5
Measured (*left*) and calculated diffuse scattering (*right*) of the disordered single-crystal sample of the $hP386$-Al$_{57.4}$Cu$_{3.6}$Ta$_{39.0}$ structure. The shown reflections correspond to the reconstruction of the $h0l$ plane of the reciprocal space pattern. Some additional reflections are due to an additional crystalline individual in the sample. The insert shows an enlarged part of the diffraction pattern for better visibility of the diffuse streaks.

Figure 6
Measured (*left*) and calculated diffuse scattering (*right*) of the disordered single-crystal sample of the $hP386$-Al$_{57.4}$Cu$_{3.6}$Ta$_{39.0}$ structure. The shown reflections correspond to the reconstruction of the $h5l$ plane of the reciprocal space pattern. Some additional reflections are due to an additional crystalline individual in the sample. The insert shows an enlarged part of the diffraction pattern for better visibility of the diffuse streaks.
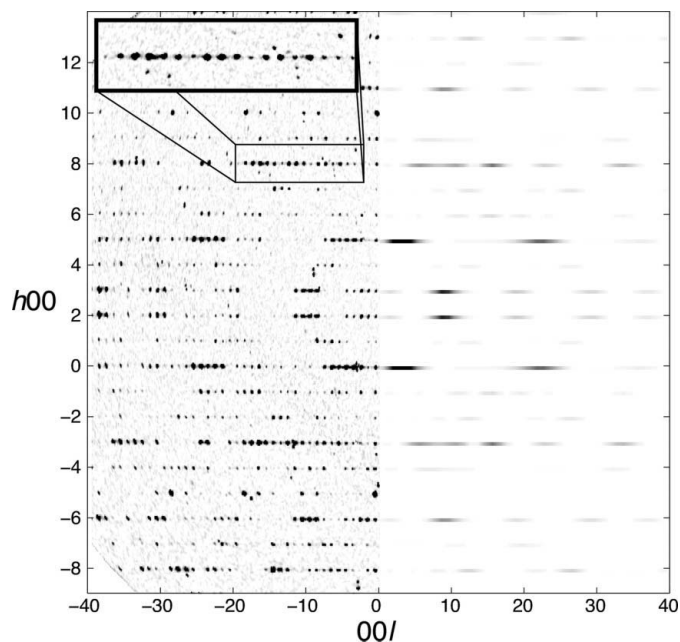
---

projection onto the (110) plane, all heavy atoms cluster around 0, 0, z and 1/3, 1/3, z. Perpendicular to this plane, *i.e.* in the **c** direction, the position of the heavy atoms depends on the choice of average structure. In the case of $c_B = c/28$, the heavy atoms lie in the $x, y, 0$ plane. In the case of $c_B = c/14$ the heavy atoms are projected around $x, 1/2, 0$ and $x, 0, 1/2$ forming a basic structure of the $hP3$-AlB$_2$-type. The light atoms are scattered over a rather large region around these sites.

5.2. Layer description

If a structure can be described as cubic or hexagonal close-packing (c.c.p./h.c.p.) of clusters, a layer structure should also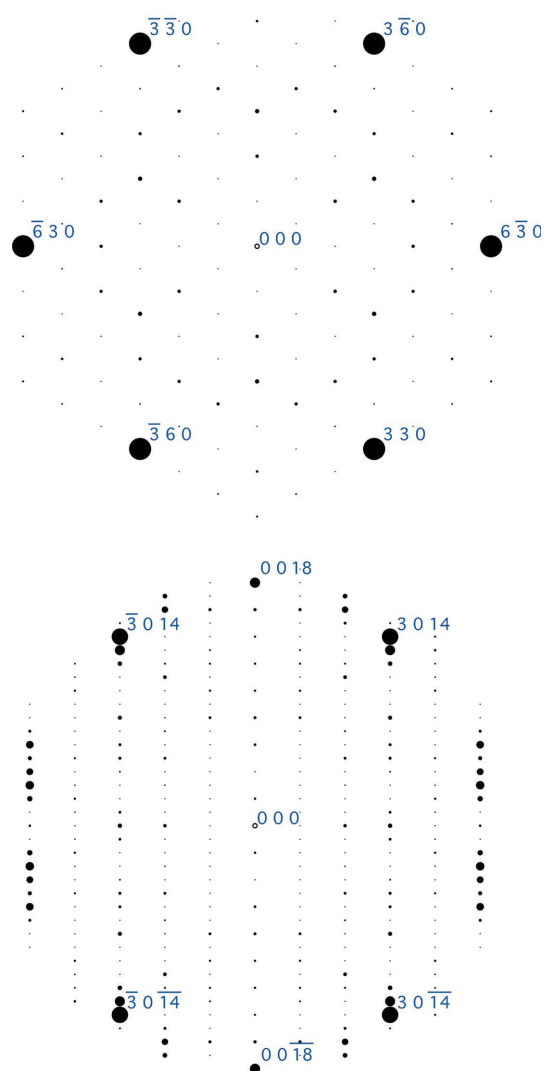 result on an atomic scale. Conversely, since many simple metallic structures – such as the basic structures of such complex compounds – can be described as layered structures, a description of the superstructure should work along the same lines. The stacking should be analogical and simply contain correspondingly modulated layers.

The layer structure of $cF444$-Al$_{63.6}$Ta$_{36.4}$ and other related structures was previously analyzed as being a repetition of three {110} layers, two of which are symmetrically inequivalent (Dshemuchadse *et al.*, 2011). A flat layer – located on a mirror plane – is succeeded by two puckered layers, related to one another by a glide plane. This stack is then translated and repeated. This three-dimensional system of {110} layers was previously visualized in a projection of the structure along the [001] direction (Dshemuchadse *et al.*, 2011). It can also be observed when projecting in the [111] direction, where part of the three-dimensionally entwined system of layers becomes visible.

The structure of $hP386$-Al$_{57.4}$Cu$_{3.6}$Ta$_{39.0}$ discussed here exhibits similar layers. The {110} layers can be best visualized in a projection on the (001) plane, as shown in the top of Fig. 9. However, due to a different crystallographic basis, the rest of the layer system is harder to recover.

Figure 7
Simulated diffraction patterns of $hP386$-Al$_{57.4}$Cu$_{3.6}$Ta$_{39.0}$ with the ($hk0$) plane at the *top* and the ($h0l$) plane at the *bottom*. The peak intensity is proportional to the diameter of the circle representing each Bragg reflection. The strongest peaks are 330, 00$\overline{18}$, and 30$\overline{14}$, and their symmetry equivalents.
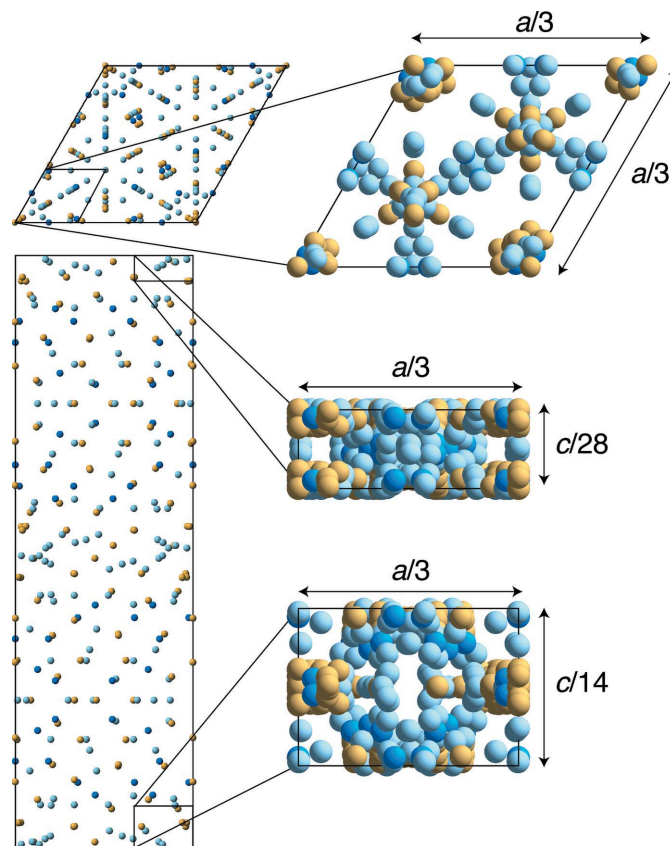

Figure 8
Projected unit cell of $hP386$-Al$_{57.4}$Cu$_{3.6}$Ta$_{39.0}$ (*left*) and its average structures (*right*). At the *bottom right*, projections of the two variants of the average structure are shown.

A more direct comparison between the cubic and hexagonal structures can be drawn if the cubic structure is transformed. For this, the face-centered cubic structure $cF444$-$Al_{63.6}Ta_{36.4}$ was first returned to its primitive representation with a rhombohedral unit cell. The unit-cell parameter $a = b = c$ of the new unit cell is $a = a_{cubic} \times 1/2^{1/2} = 13.553$ Å [$a_{cubic} = 19.1663$ Å (Weber *et al.*, 2009), $\alpha = \beta = \gamma = 60°$]. Subsequently, the rhombohedral cell is again transformed into a rhombohedrally centered hexagonal unit cell $hR333$ with lattice parameters $a = a_{cubic} \times 1/2^{1/2} = 13.553$ Å and $c = a_{cubic} \times 3/3^{1/2} = 33.197$ Å. The respective transformation matrices are given in the *Appendix*. The stacked layers in the $cF444$ unit cell all have {110} orientations, *i.e.* (110), (1$\bar{1}$0),
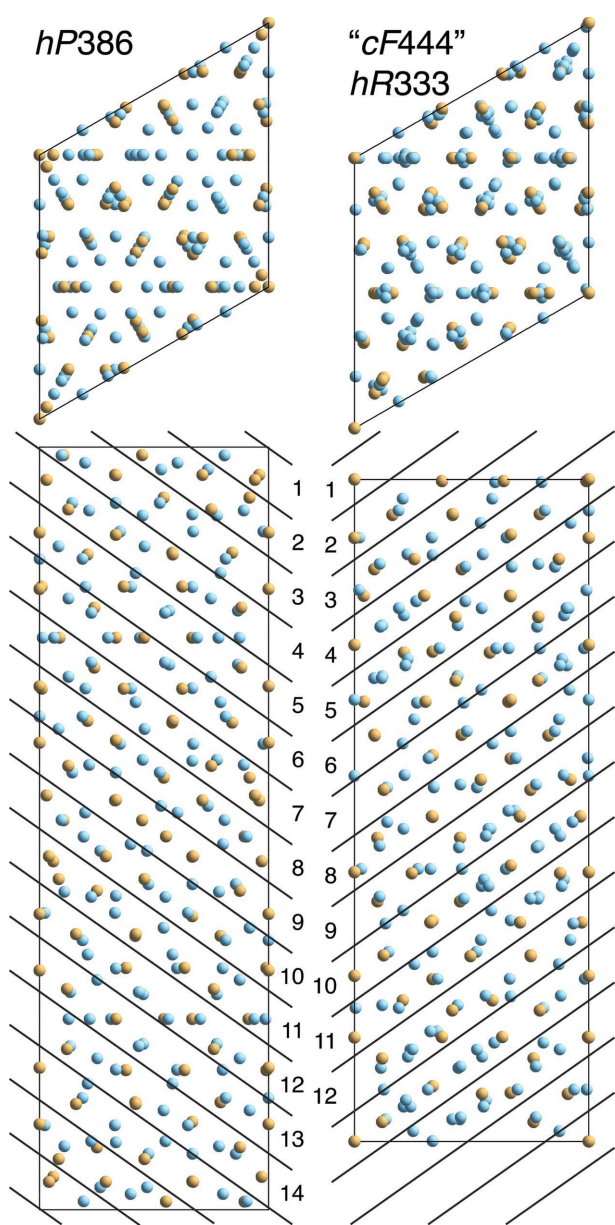
(1̄0$\bar{1}$), (1̄01), (011), (01$\bar{1}$). In the new hexagonal setting, these correspond to ($\frac{1}{2}$02), ($\frac{1}{2}\bar{1}$0), (0$\frac{1}{2}\bar{2}$), (1̄$\frac{1}{2}$0), ($\frac{1}{2}\frac{1}{2}$2), ($\frac{1}{2}\frac{1}{2}$0).

The resulting a parameter is comparable to the one determined for the hexagonal unit cell ($a = 13.512$ Å), while the c parameter differs tremendously in the hexagonal case ($c = 39.022$ Å). A comparison of the two hexagonal unit cells is shown in Fig. 9. The projections along the **c** directions reveal three systems of flat and puckered layers with 120° angles between them, which can be identified as ($\frac{1}{2}\bar{1}$0), (1̄$\frac{1}{2}$0) and ($\frac{1}{2}\frac{1}{2}$0). Marked in the projections in the respective **a** directions is one of the remaining three layer-stacking directions (($\frac{1}{2}$02), (0$\frac{1}{2}\bar{2}$) or ($\frac{1}{2}\frac{1}{2}$2)). Therein, the number of layers stacked along the **c** direction is counted, amounting to 14 layers in the hexagonal case and 12 in the transformed cubic case. These layers have the same orientation in both structures, which corresponds to the tetrahedral angles but with an elongated unit cell in the hexagonal case. The indices for the planes in the hexagonal unit cell are therefore slightly different with the same h and k values but slightly higher l indices, due to the relatively different angle of incidence.

The number of layers – 14 in the case of the $hP386$ structure – coincides with the found superstructure. In the cubic case, it can be decomposed into $12 = 3 \times 4$, where 3 is the number of different stacked layers and 4 is the number of stacks (of 3 layers each) which contained within one unit cell along the body diagonal (111) in the cubic case and accordingly along the **c** direction in the hexagonal setting.

5.3. Comparison with isostructural $hP390$-$Na_{96}In_{97}Ni_2$ and other complex intermetallics

The main cluster shells in isostructural $hP390$-$Na_{96}In_{97}Ni_2$ (Sevov & Corbett, 1993a) were already identified as fullerene-like F_{60}^{32} and F_{74}^{39}. In this compound the cluster located at $2a$ is centered by one Ni atom that is surrounded by a highly disordered In shell, containing approximately 10 atoms.[7] The second cluster shell, Na_{32}, corresponds to a fully capped pentagonal dodecahedron (distorted rhombic triacontahedron), while the third shell, $In_{48}Na_{12}$, can be described as F_{60}^{32}-fullerene, with the Na atoms on exactly the same positions as Ta in $hP386$-$Al_{57.4}Cu_{3.6}Ta_{39.0}$.

The cluster around $2c$ is also centered by a Ni atom and the first shell, containing approximately 10 In atoms, is also heavily disordered. The second cluster shell is again a FK_{39}^{74} polyhedron with its vertices all occupied by Na atoms. The third shell, a F_{74}^{39} fullerene, is made up of In atoms, only.

Obviously, and as already indicated by the different stoichiometry, there is no one-to-one correspondence between the kind of atoms on the different sites of the two otherwise isostructural compounds. This is the case to a certain extent only within the fullerene-like cluster shells. The F_{60}^{32} shell consists of 48 Al/In and 12 Ta/Na atoms, respectively, while the larger F_{74}^{39} shell exhibits Al and mixed Al/Cu positions or, on the other hand, In positions. In general, all Ta, Al and mixed Al/Cu positions in the one structure are mostly occupied by

Figure 9
Projections of the structures $hP386$-$Al_{57.4}Cu_{3.6}Ta_{39.0}$ (*left*) and $cF444$-$Al_{63.6}Ta_{36.4}$ (*right*) along the **a** and **c** directions of the hexagonal settings. The {110} layers are marked and counted along the **c** directions.

---

[7] The published coordinates are shifted by $(00\frac{1}{2})$ with respect to ours (Villars & Cenzual, 2009/10).

Na, In and again In atoms in the other structure, respectively. Different occupancies can be observed on the following sites: the atoms on the 2*a* and 2*c* positions, the atoms capping the pentagons of the second cluster shells around the 2*a* and 2*c* positions, and the atoms at the edges of one Friauf polyhedron.

Beside *hP*390-Na$_{96}$In$_{97}$Ni$_2$, there is another compound with a huge unit cell and fullerene cluster shells known in the Na–In–Ni system, *oP*742-Na$_{172}$In$_{197}$Ni$_2$ (Sevov & Corbett, 1996). Also in the binary Na–In system, a couple of complex intermetallics have been found (Sevov & Corbett, 1992; Cordier & Müller, 1993; Sevov & Corbett, 1993*b*).

Since Tl is situated directly below In in the periodic table of elements (group 13), the Na–Tl system also seems to be worth considering. The two 1:1 compounds NaTl and NaIn also form the same structure type, so Tl and In can be considered as forming equivalent intermetallic compounds with Na and perhaps also other metals. If one looks more closely into the Na–Tl phase diagram, the complex compound *cF*408-Na$_{86.3}$Tl$_{13.7}$ stands out (Samson & Hansen, 1972): it not only shares the space group with *cF*444-Al$_{63.6}$Ta$_{36.4}$, but also belongs to the same aristotype of structures (Dshemuchadse *et al.*, 2011); these structures differ by only one rhombic dodecahedron in *cF*408-Na$_{86.3}$Tl$_{13.7}$ being substituted by a Friauf polyhedron in *cF*444-Al$_{63.6}$Ta$_{36.4}$. Additionally, the atomic decoration is of course different, as can be seen directly from the different ratios between the majority and minority components in the phases. Considering the differences in composition, however, the relationship between *cF*444-Al$_{63.6}$Ta$_{36.4}$ and *hP*386-Al$_{57.4}$Cu$_{3.6}$Ta$_{39.0}$ seems to be much closer than that between *cF*408-Na$_{86.3}$Tl$_{13.7}$ and *hP*390-Na$_{49.2}$In$_{49.8}$Ni$_{1.0}$.

5.4. The complex Al–Cu–Ta system

As mentioned before, in addition to the *hP*386-Al$_{57.4}$Cu$_{3.6}$Ta$_{39.0}$ structure described here, three f.c.c. complex intermetallics are already known in the Al–Cu–Ta system. All of these four structures have very similar compositions with around 60% aluminium content and very little or no copper. Their stoichiometries are visualized in a ternary diagram in Fig. 10.

Additionally, some other phases are represented which are either known ternaries in the Al–Cu–Ta phase diagram or relevant binary phases (in the Al–Ta system). These are again labeled with their Pearson symbols. The hexagonal Laves phase was reported in the compositional range TaAl$_{1.72–0.86}$Cu$_{0.28–1.14}$ for the MgZn$_2$ structure type and is labeled *hP*12 (Nowotny & Oesterreicher, 1964; Oesterreicher *et al.*, 1965). The μ phase was reported to crystallize in the Fe$_7$W$_6$ structure type and has a unit cell *hR*39 (Nowotny & Oesterreicher, 1964). Three binary Al–Ta phases are also given: *tI*8 denoting Al$_3$Ta in the so-called 'DO$_{22}$' structure type (Condron *et al.*, 2003), *mP*86 the Ta$_{52.6}$Al$_{47.4}$ structure (Boulineau *et al.*, 2006), and *tP*30 the σ-phase Ta$_2$Al (Edshammar & Holmberg, 1960).

The cubic compounds have been previously described with the cluster approach (Conrad *et al.*, 2009) and have a couple of building blocks in common with the hexagonal compound. The most conspicuous of these are the fullerene-like three-shell clusters, which constitute the main part of all four structures in this small compositional range. The exact geometry of these fullerenes, however, differs slightly between the two different lattice symmetries. In the cubic compounds, F_{76}^{40} clusters are packed in a hierarchical way: in the structure with the smallest unit cell (*cF*444), these fullerenes are packed closely and stacked in an *ABC* manner. In the next-largest structure, however, four of these fullerenes build a close-packed tetrahedron, which is then again packed closely in an f.c.c. lattice. As if by logical consequence, the biggest of the three cubic structures (*cF*23256) exhibits a similar close-packed tetrahedron, but with edge-length three and comprising ten close-packed fullerenes. These are located on the same positions as in the previous case, again forming an *ABC* stacking. The interstices between the here-described fullerenes are filled by other structural motifs, as detailed by Conrad *et al.* (2009).

Coming back to the hexagonal structure, a close packing of fullerenes is again the first geometrical interpretation that meets the eye. The fullerenes have different shapes – F_{60}^{32} and F_{74}^{39} – and follow a different kind of stacking: *ABAC* with respect only to the positions of the cluster centers. The network between the fullerene-like clusters is built by two kinds of *FK* polyhedra in both the *cF*444 and the *hP*386 phase: FK_{16}^{28} and FK_{15}^{26}.

The network of the Ta atoms exhibits pentagonal bifrusta, which are not only found in the hexagonal structure but also in
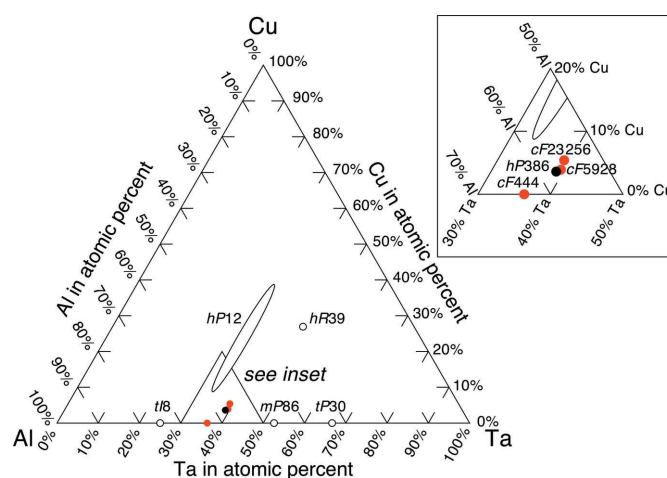

Figure 10
Ternary composition diagram of the Al–Cu–Ta system with the three f.c.c. complex intermetallics *cF*444 {*cF*444-Al$_{63.6}$Ta$_{36.4}$ (Mahne & Harbrecht, 1994; Weber *et al.*, 2009), *cF*5928 [*cF*(5928-20)-Al$_{56.6}$Cu$_{3.9}$Ta$_{39.5}$] and *cF*23256 (*cF*(23256-122)-Al$_{55.4}$Cu$_{5.4}$Ta$_{39.2}$; Weber *et al*, 2009; Conrad *et al.*, 2009; all red}, as well as the new *hP*386-Al$_{57.4}$Cu$_{3.6}$Ta$_{39.0}$ (black). In addition, the following phases are represented: the hexagonal Laves phase *hP*12, the μ phase *hR*39, and the binaries *tI*8 (Al$_3$Ta), *mP*86 (Ta$_{52.6}$Al$_{47.4}$) and *tP*30 (Ta$_2$Al, σ phase).

all three cubic compounds (Conrad *et al.*, 2009). In the same instance, hexagonal bipyramids are found in all four structures.

Since the same elements are participating in structure formation in all four cases, the common geometries are not surprising. However, even if we regard the similar building blocks as a logical consequence from small differences in stoichiometry: the radical change of the packing of those clusters in vastly different symmetries is remarkable. The exact composition, and with it the Cu content, seem to be a crucial factor determining whether the structure is face-centered cubic or hexagonal close-packed.

6. Summary

The structure of $hP386$-$Al_{57.4}Cu_{3.6}Ta_{39.0}$ was determined and interpreted with the cluster approach to describe complex intermetallics. Its composition is very close to three previously known complex intermetallic compounds in the Al–Cu–Ta system. It features two new three-shell fullerene-like polyhedra with 60 and 74 vertices.

In addition to its ordered variant, the structure was found to exist in a disordered crystal, featuring a modified structural slab that is interlaced with the ordered structure. The fullerene-like clusters in the modified slab possess 76 vertices and have previously been found in three cubic Al–(Cu)–Ta structures with very similar compositions.

Including this new hexagonal complex compound identified in the system Al–Cu–Ta, we now know altogether four variations of one packing principle of large endohedral fullerene-like clusters. With small changes in the stoichiometry, the fundamental clusters remain essentially the same, only the way of packing changes. The dominant role of geometrical factors is obvious since similar structures are observed in other systems such as In–Na–Ni, which have completely different chemical properties.

APPENDIX A
Cubic to-hexagonal transformation

For the transformation of the face-centered cubic unit cell to the underlying primitive rhombohedral unit cell, the following transformation matrix was applied

$$\begin{pmatrix} 1/2 & 1/2 & 0 \\ 0 & 1/2 & 1/2 \\ 1/2 & 0 & 1/2 \end{pmatrix}. \qquad (1)$$

The subsequent transformation from a rhombohedral unit cell with $a = b = c$ and $\alpha = \beta = \gamma \neq 90°$, the following matrix was used

$$\begin{pmatrix} 1 & \bar{1} & 0 \\ 0 & 1 & \bar{1} \\ 1 & 1 & 1 \end{pmatrix}. \qquad (2)$$

References

Boulineau, A., Joubert, J.-M. & Černý, R. (2006). *J. Solid State Chem.* **179**, 3385–3393.
Condron, C. L., Miller, G. J., Strand, J. D., Bud'ko, S. L. & Canfield, P. C. (2003). *Inorg. Chem.* **42**, 8371–8376.
Conrad, M., Harbrecht, B., Weber, T., Jung, D. Y. & Steurer, W. (2009). *Acta Cryst.* B**65**, 318–325.
Cordier, G. & Müller, V. (1993). *Z. Kristallogr.* **205**, 306–308.
CrystalMaker Software Ltd (2009). *CrystalMaker.* CrystalMaker Software Ltd, Oxford, UK.
Dshemuchadse, J., Jung, D. Y. & Steurer, W. (2011). *Acta Cryst.* B**67**, 269–292.
Edshammar, L.-E. & Holmberg, B. (1960). *Acta Chem. Scand.* **14**, 1219–1220.
Frank, F. C. & Kasper, J. S. (1958). *Acta Cryst.* **11**, 184–190.
Kabsch, W. (1993). *J. Appl. Cryst.* **26**, 795–800.
Mahne, S. & Harbrecht, B. (1994). *J. Alloys Compd.* **203**, 271–279.
Nowotny, H. & Oesterreicher, H. (1964). *Monatsh. Chem.* **95**, 982–989.
Oesterreicher, H., Nowotny, H. & Kieffer, R. (1965). *Monatsh. Chem.* **96**, 351–359.
Palatinus, L. & Chapuis, G. (2007). *J. Appl. Cryst.* **40**, 786–790.
Samson, S. & Hansen, D. A. (1972). *Acta Cryst.* B**28**, 930–935.
Sevov, S. C. & Corbett, J. D. (1992). *Inorg. Chem.* **31**, 1895–1901.
Sevov, S. C. & Corbett, J. D. (1993a). *Science,* **262**, 880–883.
Sevov, S. C. & Corbett, J. D. (1993b). *J. Solid State Chem.* **103**, 114–130.
Sevov, S. C. & Corbett, J. D. (1996). *J. Solid State Chem.* **123**, 344–370.
Sheldrick, G. M. (2008). *Acta Cryst.* A**64**, 112–122.
Simonov, A., Weber, T. & Steurer, W. (2013). In preparation.
Steurer, W. (2006). *Philos. Mag.* **86**, 1105–1113.
Villars, P. & Cenzual, K. (2009/10). *Pearson's Crystal Data.* Ohio, USA: ASM International.
Weber, T., Dshemuchadse, J., Kobas, M., Conrad, M., Harbrecht, B. & Steurer, W. (2009). *Acta Cryst.* B**65**, 308–317.